3D in situ observation of the capillary infiltration of molten silicon in a SiC/SiC composite by X-ray tomography

H. Carpentier, G. Couégnat, O. Caty, A. King, Y. Le Petitcorps, Eric Maire, A. Marchais, N. Eberling-Fux

3D in situ observation of the capillary infiltration of molten silicon in a SiC/SiC composite by X-ray tomography

H. Carpentier[a,b,*], G. Couégnat[a], O. Caty[a], A. King[c], Y. Le Petitcorps[a], E. Maire[d], A. Marchais[b], N. Eberling-Fux[b]

[a] LCTS (Univ. de Bordeaux/CNRS/CEA/SAFRAN CERAMICS), 3 allée de la Boétie, F-33600, Pessac, France
[b] SAFRAN CERAMICS, F-33185, Le Haillan, France
[c] Synchrotron SOLEIL, F-91192, St-Aubin, France
[d] Université de Lyon, INSA-Lyon, MATEIS CNRS UMR5510, 7 Avenue Jean Capelle, F-69621 Villeurbanne, France

[*] Corresponding author. LCTS (Univ. de Bordeaux/CNRS/CEA/SAFRAN CERAMICS), 3 allée de la Boétie, F-33600, Pessac, France. E-mail address: carpentier.hugo.research@gmail.com (H. Carpentier).

Abstract

The Liquid Silicon Infiltration (LSI) process is used to decrease residual porosity of SiC/SiC composite materials. However, it is not fully mastered since the mechanisms involved at 1500 °C under high vacuum are complex to analyze, especially without direct observation. Previous work had demonstrated the feasibility of using X-ray radiography to observe the front rise of silicon in a SiC/SiC composite material during the LSI process. 2D observations, as a first approach, could give a basic understanding of the mechanisms but raised several interrogations due to the superposition of these phenomena along the thickness preventing any quantification. The setup has been improved in order to make X-ray tomography using a fully integrated DC motor in place of the rotation stage commonly used. The sets of X-ray tomographs confirm two successive fillings. First, the molten silicon rapidly and non uniformly invades the accessible intergranular micro porosity of the powder. Then, the liquid slowly fills the remaining isolated powder areas. Once the SiC matrix is fully saturated, the liquid fills the bigger porosities such as cracks and intra yarn macro porosities. In addition, this 3D analysis enabled to give a better comprehension of the non uniform wetting front in the SiC matrix powder. During the 1st step, the accessibility of the powder was known to have a major effect on the speed of progression. Also, the cracks network plays a key role in the filling of the isolated areas in the powder matrix.

Key words : X-ray, tomography, 3D, in situ, capillary, infiltration, high vacuum, high temperature, Liquid Silicon Infiltration, Melt Infiltration, molten, silicon.

1 Introduction

Due to environmental restrictions, the aeronautical industry had to develop more efficient engines. In order to increase its performance, the combustion must take place at higher temperature meaning that the parts and components need to resist extreme conditions such as a corrosive, oxidant and high temperature atmosphere. To meet these requirements, a special interest has been focused on $SiC_{fibers}/SiC_{matrix}$ ceramic matrix composites (CMC) materials. SiC materials are used in many applications because it is a low density material with interesting structural, electrical and thermal properties [1, 2, 3].

The main challenge is to elaborate such materials without residual porosity. The SiC/SiC CMCs can be elaborated by means of ceramic process (suspension of SiC powder), gaseous process (Chemical Vapour Infiltration), or liquid process (Polymer Impregnation and Pyrolysis/ Reactive Melt Infiltration). The combination of these techniques followed by the capillary infiltration of silicon inside the remaining porosities (Liquid Silicon Infiltration : LSI or Melt Infitlration : MI) is the most promising approach to achieve dense composites. It has the large benefit of being pressureless and hence energy efficient.

Yet, some areas remain unfilled after the LSI process and the mechanisms occuring at high temperature, above the silicon melting point (1414 °C) are not fully understood. For a better comprehension, a growing industrial interest in monitoring this step is born at the end of the 1990's with the General Electric (GE) research center [4]. Einset first developed a setup able to follow the silicon front with thermocouples inside the composite measuring the temperature jumps during the exothermic Reactive Melt Infiltration (RMI) [5]. Later on, several devices were invented to measure the mass or the height of liquid during the capillary rise [6, 7, 8]. These works could reveal that the capillary rise of silicon inside homogeneous SiC compact powder materials follows the modified Washburn law. This law enables to extract an effective diameter that represents the pore structure of the medium. It increases with the speed of infiltration which makes it an interesting and convenient kinetic parameter when it comes to comparing the infiltration of different samples. Pratically, the effective diameter is computed from Washburn experiments at room temperature with organics solvents as it is independent of the fluid characteristics. It is then useful to predict kinetics at high temperature where Washburn experiments are more difficult to manage [9]. Although these kinetic information are important and give an insight into the quality of filling, it is also necessary to make ex situ characterisation to understand the progression of the fluid inside the porous medium. Marchais, could hence demonstrates that in a SiC/SiC composite, the silicon first invades the intergranular micro porosity of the matrix at a rate close to 0.4 mm/sec and then fills the larger scale porosities such as shrinkage cracks and intra yarns macro porosities [7]. This two step mechanism of filling could also be confirmed by the two slopes obtained by the Washburn experiments during the LSI process of heterogeneous SiC compact powder materials [10]. Until recently, no in situ observation had been made of the LSI process, leaving unanswered interrogations about the transfer of liquid silicon between the different components of the composite or the reason why some areas remain unfilled at the end of the LSI process.

Thankfully, major progress have been made in the field of in situ experiments using X-ray synchrotron radiation. For instance, the microstructure evolution has been imaged during axial impregnation of unidirectional ceramic fibre beds and pyrolysis of a SiC-based preceramic polymer up to 1200

°C [11, 12, 13]. A large number of experimental setup have been developed for synchrotron X-ray in situ observation [14, 15, 16, 17, 18, 19] which led us to adopt a new approach for the understanding of the capillary infiltration during the LSI process. In our previous work, a setup was developed to observe the capillary rise of molten silicon in a SiC/SiC composite with X-ray synchrotron radiation. It could confirm both the sequence of filling in the composite and the speed of infiltration inside the SiC powder matrix [20]. Based on radiographs, it could appear that bigger porosities take more time to fill and the comprehension of the liquid progression inside these areas remains incomplete, mainly due to the lack of 3D information.

The present work aimed at giving a 3D observation of the LSI process using high speed micro computed tomography (μCT) with in situ information of the filling in a multi components material such as a SiC/SiC composite. As well as confirming the mechanisms discussed in the literature, the main purpose is to catch phenomena that could not be understood without a full 3D tomographic observation.

The paper will first present the materials and the setup improvements to make fast tomographic observations possible at 1500 °C under high vacuum. Then, the image treatment methodology used for data analysis will be detailled. Finally, capillary infiltration mechanisms extracted from the tomographic observations will be proposed and discussed.

2 Materials and methods

2.1 Materials

In this study, SiC/SiC composites manufactured by Safran Ceramics were used. The fabrication followed the Slurry Cast process [21]. A BN coated-fibre SiC preform is first consolidated with SiC by Chemical Vapour Infiltration (CVI). Each yarn is approximately composed of 500 fibres Hi-Nicalon S and the weave is of type 2D interlock with longitudinal rectilinear yarns and transverse tortuous yarns woven through several layers. Then, the preform is injected with the slurry, an aqueous suspension of SiC powder, resulting in the matrix.

Afterwards, it is dried which may lead to the formation of shrinkage cracks in the SiC matrix. Lastly, rectilinear samples of height 100 mm and of cross section 2.5×2.5 mm^2 are machined from the SiC plate. This design was chosen to meet a 4.5 µm spatial resolution with full section observation.

The samples were thermally treated to bind the SiC particles together and remove non wetting barriers before final Melt Infiltration step prior to the infiltration process. The thermal treatment lasts 14 h at 1400 °C under high vacuum. The liquid used was a silicon-boron alloy to prevent excessive reactive infiltration.

The initial state of the material is presented in Supplementary Fig. S1 (Soleil μCT, method described in section 2.2.4). Before infiltration the difference between yarns and compact powder is visible even if the quality of the tomograph is not as good as the one obtained on a laboratory tomograph. Porosities can be clearly identified, especially cracks in the matrix. A porosity analysis revealed that the major connected porosity is located between the yarns and the matrix (yarn/matrix decohesions).

2.2 Methods

2.2.1 Material characterization before synchrotron experiment

Pore size distribution and porosity were measured by mercury intrusion porosimetry (Autopore IV, Micromeritics Instrument Corp., USA) for a sample volume of 0.7 cm^3.

Capillary infiltration experiments were performed on a modified commercial tensiometer (Tensio-Cad W TE-5200 MO, CAD Instrument, France) operating at 20 °C in a temperature regulated room. Hexadecane was used as a solvent for its low volatility (saturation vapor pressure : 4.88×10^{-2} Pa). This experiment is repeatable and non destructive.

2.2.2 High temperature infiltration device for in situ observation

In a previous work, a specific Neyco vacuum chamber had been designed for the in situ silicon infiltration observation [20]. A high vacuum was guaranted to prevent any oxidation of the SiC/SiC sample or silicon since a small layer of SiO_2 is sufficient to prevent the wetting and hence block the infiltration [22]. The high vacuum is ensured by a turbo pump (HiCube 80 Pffeifer). Moreover, an induction coil linked to a Fives Celes generator was integrated in order to reach a high temperature (up to 1600°C) which is necessary for capillary infiltration of silicon that melts at 1414 °C. The temperature stability and homogeneity was ensured thanks to a controller linked to a thermocouple in the susceptor. A thermal cartography of the oven, with an additional thermocouple replacing the sample, was performed before any experiments to know precisely the temperature. The sample displacement was achieved with the Neyco Z translator allowing a 50 ± 0.1 mm vertical movement, sufficient to make a 5 mm deep contact between the sample and the melt. The sample fixation length, the melt height (30 mm) and the distance between the observed area and the bottom of the samples (35 mm) were kept constant throughout all experiments [Fig. 1]. The instrumentation was controlled and real time monitored by a customized python application.

The strong point of this compact setup is its adaptability on a synchrotron tomograph base plate. Two windows made of Kapton tape are dedicated to the X-ray visualization, ensuring a low absorption and a high vacuum. However, it is not possible to use the classic rotation stage to make tomography due to the complexity of rotating the whole device. One way of solving this, was to integrate a vacuum compatible micromotor inside the heating vacuum chamber. The DC brushless motor 3056k 024B by Faulhaber was used based on the experience of Francisco García-Moreno with very fast in situ studies [15, 16]. Initially, this motor is designed to work precisely at very high speed. To satisfy the speed target of our application 100 rpm while ensuring a good precision, a gearbox had been added in our previous work [20] but it induced too much spatial irregularities, making the 3D reconstruction impossible. The main improvements of the setup were actually to remove the planetary gearheads as well as making a rigid assembly by sticking the sample to a part screwed to the rotating part to prevent any unwanted motion [Supplementary Figs. S2 and S3].

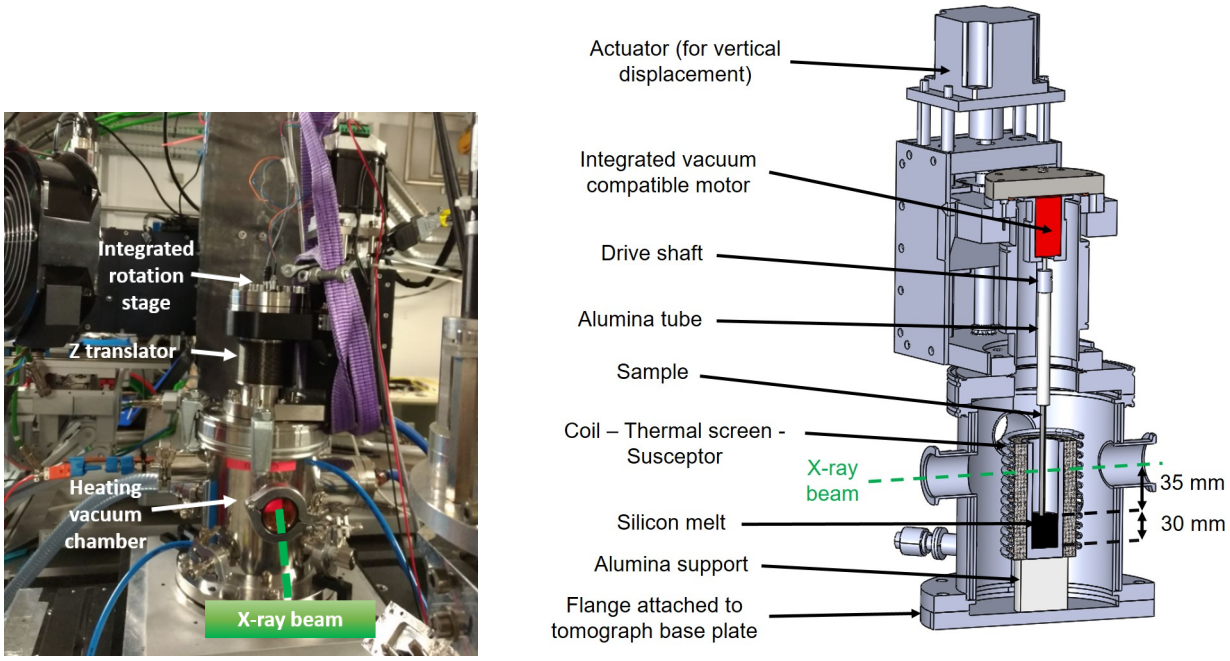

(a) Device on Soleil synchotron beamline.

(b) Annotated 3D CAD representation.

Fig. 1: General description of the heating vacuum chamber for capillary infiltration.

2.2.3 Experimental conditions

After 1 hour of vacuum pumping, reaching 10^{-3} mbar, both the sample and the melt are heated up to 1400 °C at 10 °C/min for 1 hour to homogenize the temperature and remove wetting barriers. Then, the infiltration occurs at 1500 °C after 30 minutes of heating to melt the silicon alloy. During this cycle, the sample is kept at a safety distance of 2 cm from the melt to prevent early infiltration. Then, the sample is lowered at 1 mm/s until the liquid position has been reached. Every sample mentioned hereinafter has been observed under the same experimental conditions.

2.2.4 X-ray acquisition

High-speed synchrotron tomography was performed at the PSICHE beamline of the SOLEIL synchrotron source. The imaging detector used a PCO Dimax HS4 high speed camera, coupled to a scintillator using a Hasselblad tandem objective giving an optical magnification of 2.4x. The camera sensor has 11 micron pixels, resulting in an effective pixel size of 4.5 microns. A field of view of 5.4 x 2.7 mm^2 was used, leading to 3D datasets of dimensions 5.4 x 5.4 x 2.7 mm^3. The X-ray setup operated at an average photon energy of around 30 keV, with a photon flux of 1.5E12 photons/s/mm2. Approximately 900 projections were captured over 180 degrees, each with a radiograph exposure time of 0.3 ms. Continuous rotation of the sample was achieved using the experimental setup's motor. As mentioned in the literature, the infiltration was expected to take place in two steps. Therefore, one of the main challenge at Soleil was to record the complete infiltration without saturating the onboard

camera memory (36 GB) corresponding to a maximum of 68 sets of projections. To cope with these limitations, two acquisition modes were chosen :

1. Fast Acquisition (FA) : 1 tomograph / 0.5 s continuously (2 samples) ;
2. Slow Acquisition (SA) : 1 tomograph / 0.5 s every 10 s (5 samples).

As the second filling was reported to be slower, a combination of the two modes was done on 3 samples to catch the front at high speed whereas the larger scale porosities filling was recorded at lower temporal resolution. In total, 10 samples were observed with 60 tomographs each.

2.2.5 Data analysis

The standard post processing tools available at Soleil, `tomodata`[1], were used to correct flat field, ring artefacts and add a paganin filter [23, 24]. In this particular setup, a special correction of the tomographs had to be made in order to correct the "star-shaped" artefacts. Indeed, the temporal irregularities, even small, affect the image quality [Supplementary Fig. S3].

It was found that this rotation stage required an addition correction due to a slight periodic variation in the rotation speed during a rotation. As a result, the angular increment between projections was not constant, as it is normally the case. This resulted in characteristic "star-shaped" artefacts, which increased in size with distance from the rotation axis. It was determined that the speed variation was periodic, and that the main component had a frequency of twice the rotation frequency. Thus, the angular position (ω) of projection n could be described as :

$$\omega_n = n\Delta_\omega + A\sin(2n\Delta_\omega + c) \tag{1}$$

Where A is the amplitude to the correction, and c is an angular offset. The resulting angular positions were used in PyHST2 [25] in place of the habitual constant angular increment (Δ_ω). The two parameters (A and c) were determined for a single volume in each time series by trial and error, by reconstructing series of tomographic sections using different pairs of values, and then iterating towards the optimal correction. Once the optimum values had been determined, the correction could be applied to all tomographs of a series. This required first determining the angular offset between the tomographs in the series, relative to the volume used to determine the correction. The correction was then applied to all volumes by adjusting c according to the angular offset. It was found that for rotation speeds around 360° / s, the value of A was close to 1°.

The corrected volumes were then registered with respect to their initial state to facilitate the further observation of the infiltration front. Indeed, the samples underwent continuous rotation during liquid silicon infiltration. It resulted in each scan capturing the sample at a slightly different orientation. To address this challenge, a first rigid alignment was performed using the `registration` module of `scikit-image` [26]. This step effectively compensated for these rotational shifts, ensuring better alignment for the subsequent DVC registration. Improved alignment, in turn, led to better convergence and overall accuracy of the DVC analysis accomplished thanks to an in-house digital volume correlation

[1] https://gitlab.com/soleil-psiche/tomodata

(DVC) library named `kintsugi`[2]. Under the assumption of brightness conservation, a displacement field $u(x)$ is sought that is generated by an affine deformation and that minimizes the norm of the correlation residuals $\eta(x)$ between a reference image $f(x)$ and a deformed one $g(x)$.

$$\eta(x) = f(x) - g(x + u(x)) \tag{2}$$

The displacement field is decomposed over continuous basis functions, which can be conveniently obtained using a finite element mesh as a support, hence following the so-called global DVC approach [27]. In an ideal case, the residuals should be identically zero if the brightness conservation is fully satisfied. At least, they are expected to be small with respect to the dynamic of the images, and only related to the image noise. In our particular case, the local gray level of the images are anticipated to change drastically with the progressive infiltration of the silicon, resulting in possibly large local values of residuals. This could lead to difficulties for the DVC problem to converge as these variations could not be corrected solely with a kinematic assumption. To alleviate this problem, the brightness conversation is relaxed by introducing an additional correction term [28] to the deformed image as:

$$\tilde{g}(x) \equiv g(x + u(x)) + (a_0(x) + a_1(x) \cdot f(x)) \tag{3}$$

that could accommodate local variation of the gray level, extrinsic to the displacement of the specimen. Now, both $u(x)$ and $a(x)$ are sought to minimize the generalized residuals:

$$\tilde{\eta}(x) = f(x) - g(x + u(x)) + (a_0(x) + a_1(x) \cdot f(x)) \tag{4}$$

The residuals related to the infiltration could eventually be obtained as the difference between the kinematic-corrected image $g(x + u(x))$ and the reference state $f(x)$.

This approach yielded better results (smaller residuals) compared to using a rigid transformation alone, allowing for homogeneous deformation of the sample. The apparent volume change could potentially be attributed to swelling caused by the infiltration of silicon [Supplementary Fig. S4]. However, the fast acquisition speed may have introduced reconstruction artefacts that could also contribute to the observed volume changes. While the DVC demonstrates potential for measuring sample local deformation, limitations in image quality and resolution hinder full-field strain analysis at the microstructural level. A more detailed investigation using higher resolution would be necessary for confidently measuring local strains, presenting a promising avenue for future work. Despite not fully utilizing DVC for registration, its ability to handle brightness and contrast variations was crucial in this study due to the significant local gray value variations within the samples.

3 Results

3.1 Pore size distribution and infiltration kinetics at room temperature

Prior to the LSI process, a multi scale porosity was noticed in the SiC/SiC composites as revealed by the mercury intrusion experiments conducted on three samples [Fig. 2a]. The 300-400 nm peaks are attributed to the inter granular micro porosity of the SiC powder matrix whereas the peaks in the

[2] https://gitlab.com/gcouegnat/kintsugi

range of [50-600] µm refer to the intra yarn porosities, drying cracks and macropores [Fig. 2a]. The median pore diameter varies from 648 to 1910 nm, depending on the amount of macroporosities in the sample.

In order to predict infiltration kinetics at high temperature, Washburn experiments were carried out on these samples [Fig. 2b]. Fig. 2b clearly shows two different speeds of ascension. Based on previous data [20, 29, 10, 30], the first regime can be linked to the filling of the inter-grain porosity whereas the second refers to the saturation of larger scale porosities such as intra yarn porosities, cracks, decohesions and macropores [Supplementary Fig. S1(a)]. One can notice that both the pore sizes and the Washburn effective diameters are slighlty bigger than in our previous work which is consistent with the longer heat treatment of the samples, resulting in larger pore sizes involving greater kinetics [29, 10, 30]. Also, it is interesting to note that every sample's porous architecture is different, leading to a distinct speeds of infiltration.

his approaDuring high temperature melt infiltration, mechanisms are expected to occur at two different speeds that can vary for all samples [29, 10]. At first, a fast filling should concern the micro porosity of the SiC/SiC composite matrix and a slow one should deal with larger porosities.

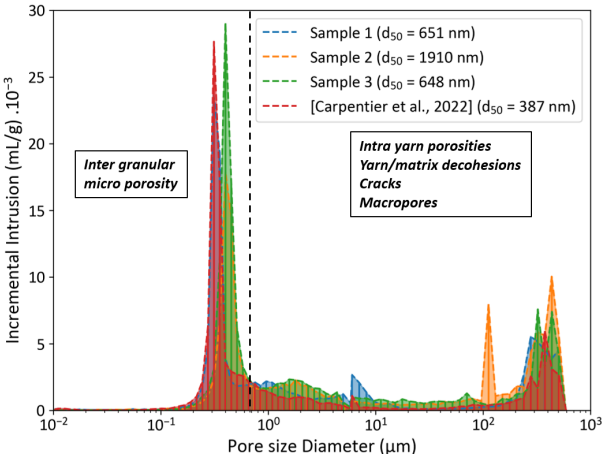

(a) Pore size distribution of SiC/SiC composites.

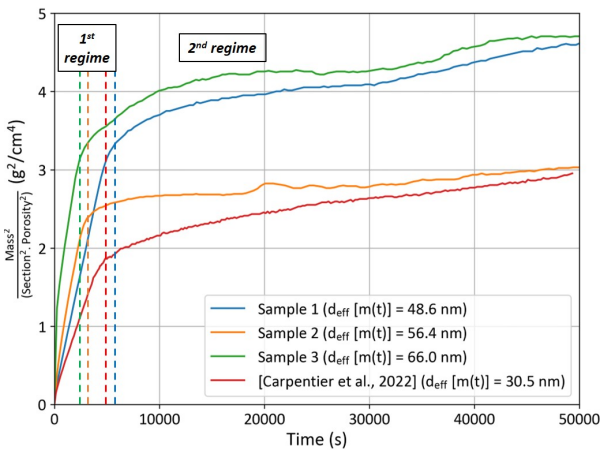

(b) Time dependence of the squared weight gain curves normalized to the section during hexadecane capillary rise.

Fig. 2: SiC/SiC composites characterization before melt infiltration.

3.2 3D in situ observation of the SiC/SiC composite filling : sequence and mechanisms

Fig. 3 shows 3D tomographic visualisation of the silicon infiltration obtained by a gray level segmentation. The unfilled powder exhibits much lower absorption compared to the yarns which enables to separate powder from yarns. The color scheme is centered on this threshold value, with blue representing the unfilled SiC powder and porosities at the initial state, while red indicates the SiC yarns. As infiltration progresses, the liquid induces a change in gray level, revealing the presence of silicon filling. The filling direction is from bottom to top. It first rises in the SiC powder matrix and then in the larger scale porosities such as shrinkage cracks and macroporosities.

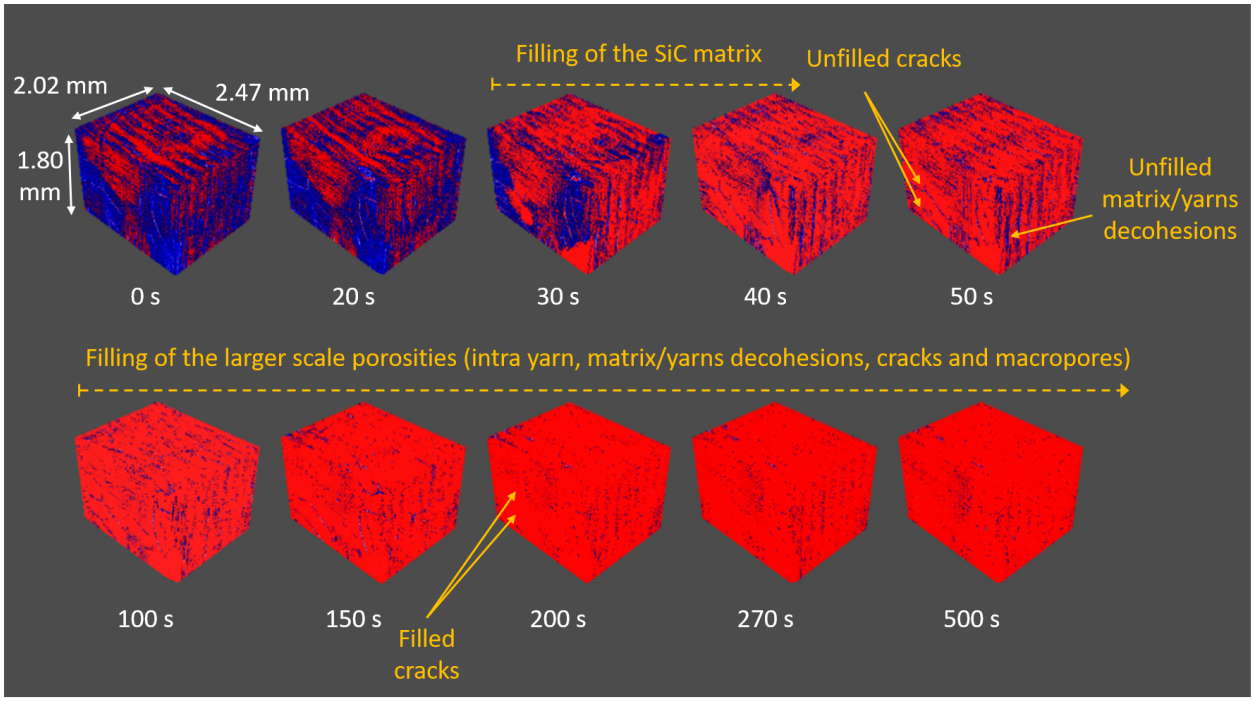

(a) 3D observations of the silicon infiltration during Slow Acquisition (SA).

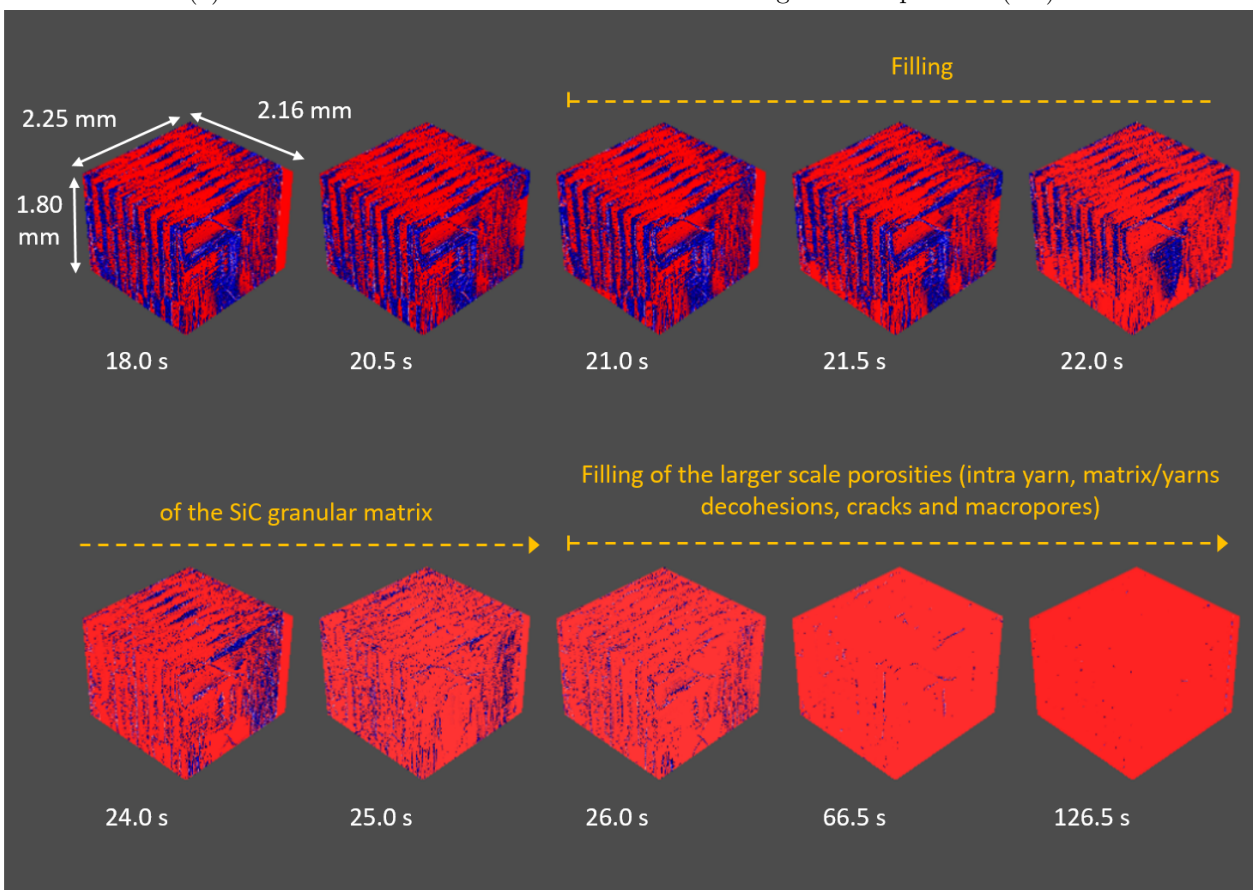

(b) 3D observations of the silicon infiltration during Fast Acquisition (FA).

Fig. 3: Confirmation of the two major steps of infiltration during Melt Infiltration.

The high temporal resolution in Fig. 3b allows for a tentative plot of porosity versus time, which is provided in the Supplementary Materials for completeness. Although the two different speeds of infiltration can be observed [Supplementary Fig. S5], the data is still too uncertain for quantitative exploitation.

These two major steps of infiltration, sensed in 2D [20], is now confirmed in 3D and can be analyzed in the volume with further details.

3.2.1 Step 1a : Vertical ascension of a non saturating silicon front in the powder matrix

The filling of the composite starts with the in plane vertical silicon ascension in the SiC powder matrix. Raw and difference images of the rising front are gathered in Fig. 4.

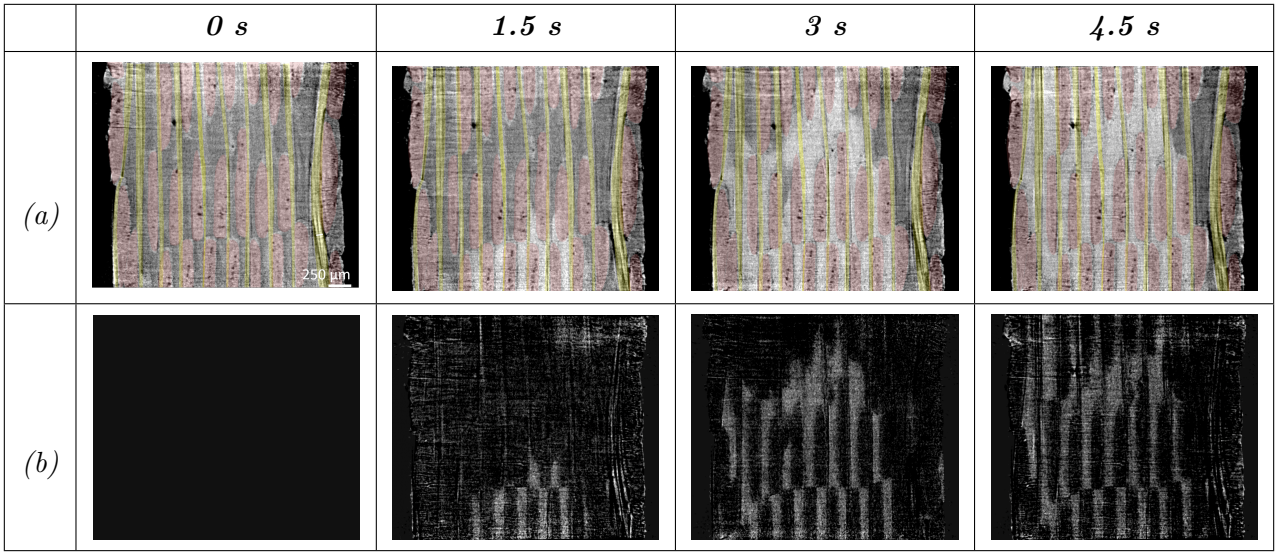

Fig. 4: Vertical ascension of the silicon non saturating front in the powder matrix - (a) Raw slices with flat field correction, (b) Difference between slices at time t and the initial state ($n_i - n_0$) to highlight the front. The longitudinal and transverse yarns are represented in yellow and red respectively, the SiC powder is gray, the porosities are black.

On the right hand side of the composite, one can see that some areas remain unfilled after the silicon vertical ascension. Indeed, step 1a does not correspond to the saturation of the whole matrix but only to a non saturating front rise. This step takes between [4.5 ; 7] s for samples observed under Fast Acquisition (FA).

3.2.2 Step 1b : Multidirectional progression of the silicon front in the powder matrix

Fast acquisitions put into light a new step and mechanism in the Liquid Silicon Infiltration process : the slower filling of the SiC matrix until full saturation thanks to a multidirectionnal progression. Raw and difference images of the saturation of the SiC powder matrix (step 1b) are gathered

in Fig. 5.

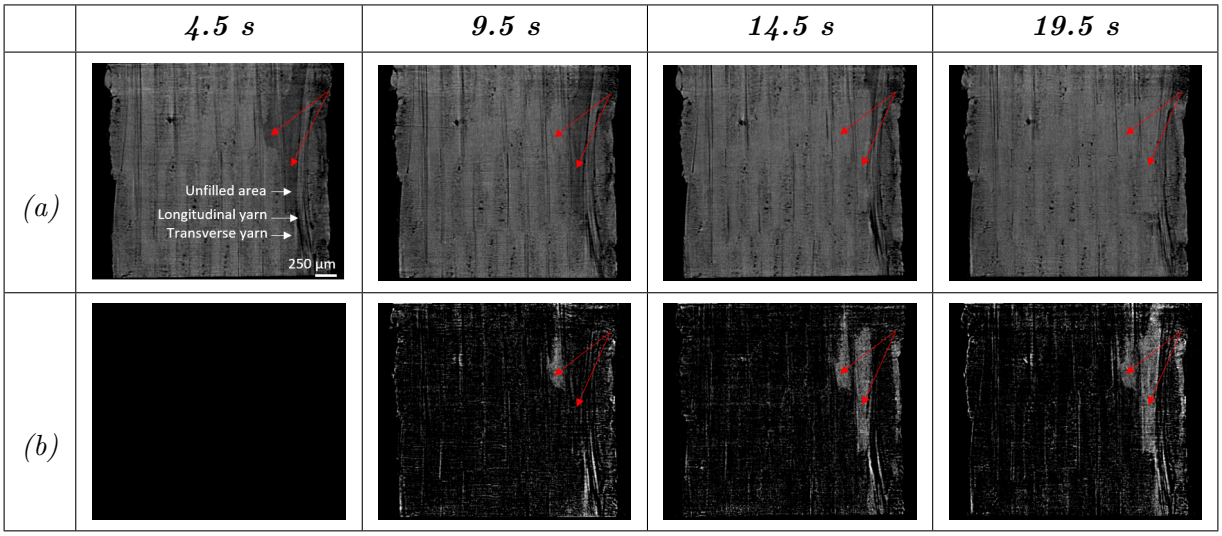

Fig. 5: Saturation of the SiC powder matrix (red arrowed) - (a) Raw slices with flat field correction, (b) Difference between slices at time t and the initial state ($n_i - n_{4.5}$) to highlight the front.

During step 1b, the progression is multi directional and does not correspond to a vertical front rise such as in step 1a [Supplementary Figs. S7, S8 and S9]. The saturation of the unfilled areas is obtained by the progression of the liquid silicon mainly coming from the decohesion yarn/matrix. This second mechanism is observed for every sample and characterizes the slower filling of step 1b.

For samples observed under fast acquisition, the accurate duration of this step is comprised between [10.5 : 12] s except for one sample where the saturation is obtained after 19.5 s from the front rise. Slower regions to be saturated are mainly powder areas located above yarns [right red arrow, Fig. 5] or above large macropores [Supplementary Fig. S9]. However, some exceptions have been observed [left red arrow, Fig. 5], it is yet to be understood.

When the SiC matrix is completely filled, the silicon starts invading every bigger porosity at the same time, marking the beginning of step 2. This second step could be split into three parts (2a, 2b and 2c) according to the type of porosities [Supplementary Fig. S10], ranked by ascending saturation time :

1. the intra yarn porosity (2a) ;
2. the cracks and the yarn/matrix decohesions (2b) ;
3. the macropores (2c).

The second step was identified in radiographs and through saturation analysis in our previous work [20]. However, determining the sequence of filling was challenging due to the unclear distinction of these larger porosities. It is now achievable with the assistance of tomography.

3.2.3 Step 2a : filling of the intra yarn porosity

Once the powder matrix is fully saturated, the filling goes on in the larger porosities of the SiC/SiC composite. Only the smallest cracks are already filled during the ascension of the silicon wetting front.

Simultaneously, the cracks, the yarn/matrix decohesions and the intra yarn porosities get filled but the latter filling is faster. It lasts between 9 s and 10.5 s for 3 samples observed at high time resolution.

A silicon liquid transfer from the matrix to the intra yarn porosity was spotted. It is made possible due to a yarn/matrix decohesion pointed out in red in Fig. 6.

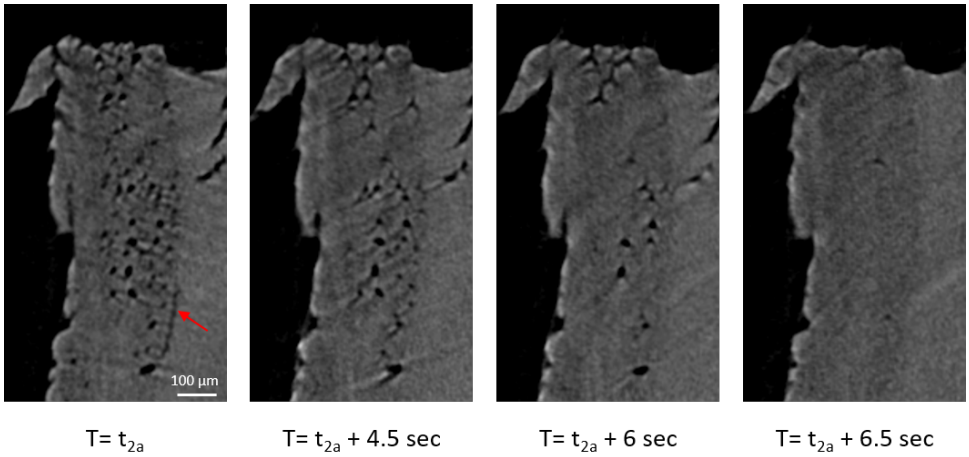

Fig. 6: Liquid transfer from the matrix to the intra yarn porosity via a yarn/matrix decohesion, the red arrow points out the yarn/matrix debonding.

It is important to mention that there is no need for all the decohesions to be completely filled to reach the intra yarn porosity saturation. The filling of the first decohesions, generally small ones, is sufficient to provide liquid silicon to the intra yarn porosities.

No front was observed in the intra yarn porosities meaning that the filling does not go from bottom to top contrary to the ascension of the front in the powder during the initial step. In the same way, the filling of transverse and longitudinal yarns takes place at the exact same time, without exhibiting a faster saturation according to a favored direction.

3.2.4 Step 2b : Filling of the cracks and yarn/matrix decohesions

The powder also needs to be filled to trigger this slower filling. For samples observed under fast acquisition, cracks and yarn/matrix decohesions are filled either in the same time or slightly after intra yarn porosities. Fig. 7 shows intra yarn porosity (white arrowed) saturated before cracks (red arrowed). The duration of step 2b varies according to the sample from 10.5 $\pm$ 0.5 s to 29 $\pm$ 0.5 s (Fast Acquisition).

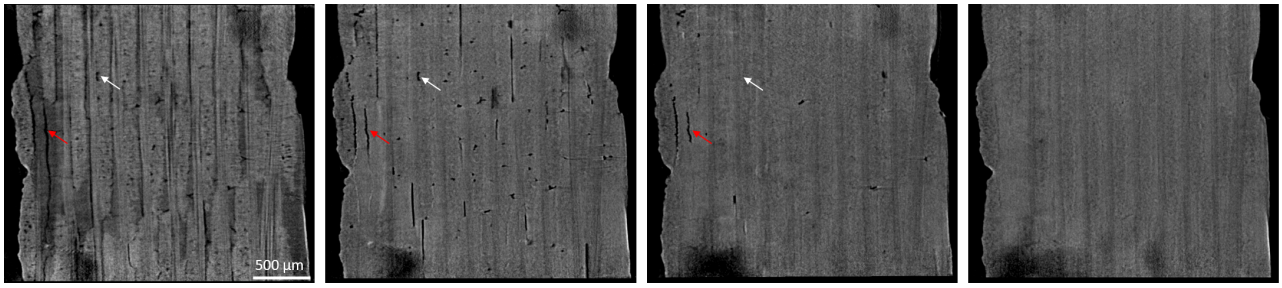

Fig. 7: Filling of the cracks ending after the saturation of the intra yarn porosities.

3.2.5 Step 2c : filling of the macropores

Step 2c constitutes the longest filling and concerns the macropores. These latter are mainly located in the matrix powder and are due to bubbles during the fabrication process (Slurry Cast). Some of them can also be the result of large yarn/matrix decohesions. Small macropores are rapidly filled whereas larger ones take more time and do not reach saturation during the aquisition [Supplementary Fig. S11]. During slow acquisitions, even after 600 seconds of Melt Infiltration, some macropores remain unfilled.

4 Discussion

Global scenario of infiltration

At room temperature, during sample characterization [Fig. 2b] and at high temperature, with in situ radiographs or weight gain monitoring during Melt Infiltration, it is now known that the filling of SiC/SiC composites takes place in two steps. However, the filling mechanisms are complex and the sequence can be decomposed in more that two steps.

At the very early moments ($\Delta t_1 < 7\ s$), the molten silicon rises non uniformly to the top of the sample inside the inter granular porosities of the SiC powder, avoiding the cracks, macro pores, intra yarn porosities and isolated powder areas [State 1a, Fig. 8]. Later on, the saturation of the SiC powder is obtained by a multi directional flow [State 1b, Fig. 8]. This newly discovered progression is made possible by the yarn/matrix decohesions that ensure the liquid transfer between already filled areas and isolated powder parts. The location of the powder matrix with respect to both the preform and the big scale porosities plays a major role in the time needed to reach saturation. The discontinuities in the SiC matrix, generated by the SiC preform and macropores, prevent the silicon from invading the medium at once and slow down the infiltration process. In addition, a few well-connected regions that saturated slowly were observed. While it is possible these regions resulted from trapped voids migrating post-saturation, as surmised by Larson et al. [12], no emptying was spotted. In Resin Transfer Molding (RTM), bubble entrapment may occur due to differential flow speeds between macro and microchannels, as discussed by Wielhorski et al. [31]. However, our study revealed successive fillings without dual fronts. Although high vacuum conditions should mitigate void formation, higher spatial resolution is advisable to rule out mechanisms identified in liquid composite molding processes [32].

As soon as the inter granular micro porosity is saturated, a second mechanism takes place with simultanously the filling of the intra yarn porosity, the cracks, the yarn/matrix decohesions and the macropores [State 2, Fig. 8]. Due to spatial superposition of the mechanisms, 2D radiographs could not clearly point out the beginning of this second slower filling. Nevertheless, 3D observations have proven that for all samples, the powder needs to be saturated to trigger the filling of larger scale porosities which could indicates that the silicon comes from the matrix. Moreover, no front was observed in this area objecting the hypothesis of a capillary ascension from bottom to top. This filling would not be the result of a Washburn classic capillary infiltration but rather the consequence of the silicon over saturation in the powder. The progression of the liquid is then multi directional which explains that no difference of speed is noticed between the transverse and the vertical longitudinal yarns [Supplementary Fig. S12]. The intra yarn porosities are saturated before the cracks and matrix/powder decohesions which has been attributed to their smaller porous volume.

The last step corresponds to the very slow filling of the macropores which could be linked to their bigger volume but also to their smaller contact surface with the silicon saturated SiC powder [State 2c, Fig. 8]. Indeed, shrinkage cracks and matrix/yarns decohesions form a major porosity network [Supplementary Fig. S1(b)] that enables a bigger supply of liquid silicon coming from the SiC matrix.

The saturation time of each component in the SiC/SiC composite varies according to the sample which can be explained by the intrinseque porosity network which is different for each sample, as it mainly depends on the manufacturing process. Nevertheless, characteristic times associated with the different filling mechanisms can still be extracted for the observed samples when considering the adequate aquisition mode (Table 1). The characteristic time values are orders of magnitude, and their determination involves a degree of manual intervention. In further work, enhanced image quality would facilitate the segmentation of images in 3D, enabling a more detailed analysis of the filling dynamics of each phase.

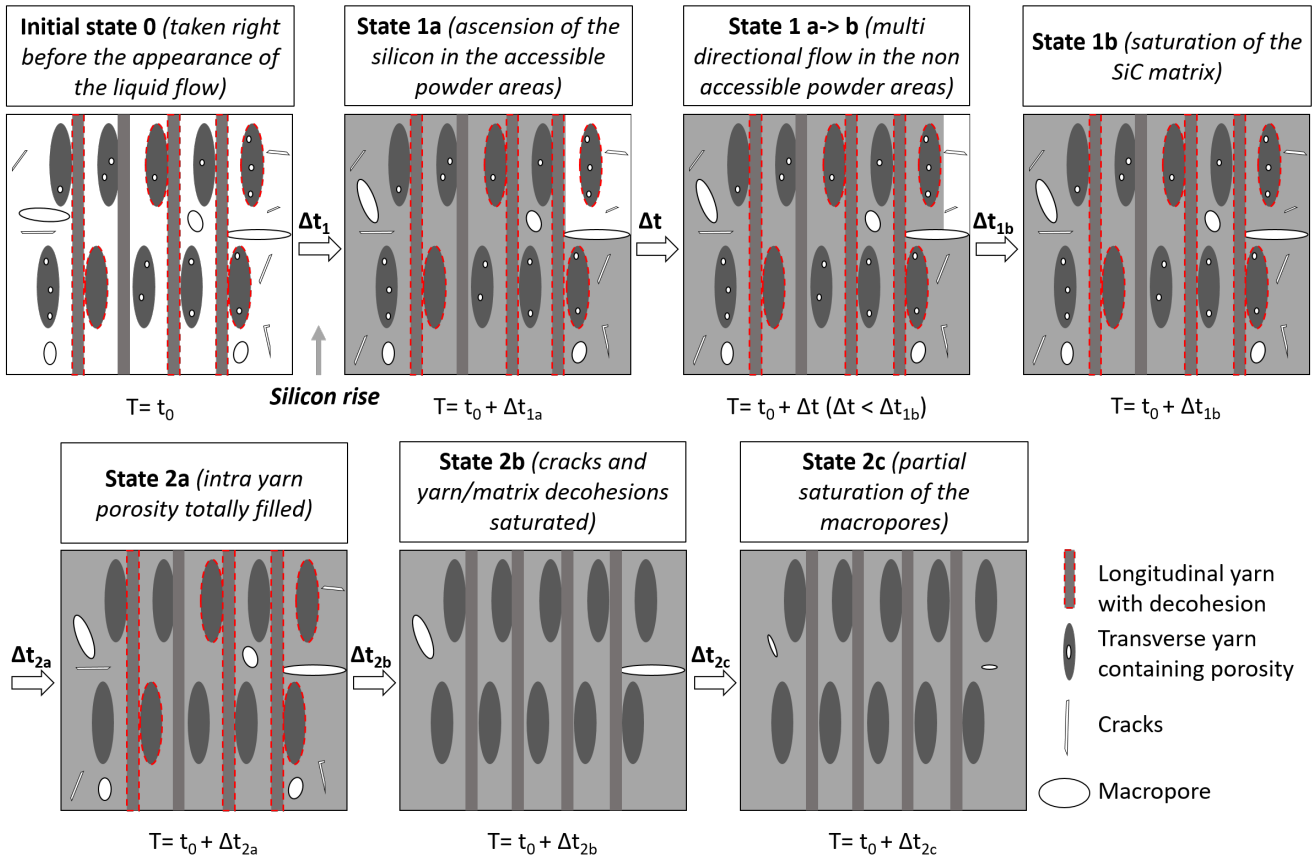

Fig. 8: Filling mechanisms of a SiC/SiC composite during molten silicon capillary infiltration.

Filling information	Duration (s) [min ; max]	Average - Standard deviation (s)
Silicon front rise in the SiC powder matrix (FA) Δt_{1a}	[4.5 ; 7]	5.5 ± 1.1
SiC powder matrix saturation (FA) Δt_{1b}	[10.5 ; 19]	13.8 ± 3.7
Intra yarn porosity filling (FA) Δt_{2a}	[9 ; 10.5]	9.8 ± 0.6
Cracks and matrix/yarns decohesions filling (FA) Δt_{2b}	[10.5 ; 29]	19.7 ± 9.2
Macropores filling (SA) Δt_{2c}	[40 ; 600]	152.5 ± 171.3

Table 1: Summary of the characteristic times associated with the different filling mechanisms.

These results highlight the importance of having volumetric information to understand the sequence of filling in a multi scale porous material such as a SiC/SiC composite. Indeed, according to Washburn theory [33], the bigger the capillary, the faster the ascension. Yet, in this work, the micro porosities located in the granular SiC matrix are filled before bigger porosities. It can be explained by the fact that these larger porosities are not directly in contact with the melt but depend on the

liquid silicon, drained by the SiC matrix. For this reason, their volume and location turned out to be key parameters in the LSI process.

5 Conclusion

A setup was developed to observe in situ and in 3D the Melt Infiltration (MI) at 1500 °C, under high vacuum thanks to synchrotron X-ray radiation. The tomographs were acquired with a 4.5 µm spatial resolution, at a rate up to 2 Hz which was a necessary compromise to capture all the fillings mechanisms taking place in the CMC specimens.

The experimental results reveal a multiple step filling mechanism of the SiC/SiC composites with two distinct speeds. At first, the liquid silicon rapidly rises inside the major part of the SiC intra granular porosity, leaving behind isolated powder areas. The wetting front is then not uniform nor saturating. It turns out that the saturation of the SiC matrix comes later with a multi directional progression of the molten alloy mainly coming from yarn/matrix decohesions. During this step, the filling time increases with the isolation of the area since it does not result from a classical Washburn infiltration but from the over saturation of already filled powder areas. It has been confirmed that only when the SiC powder matrix is fully saturated, the intra yarn porosity, shrinkage cracks, matrix/yarns decohesions and the macropores simultaneously start to fill. Macro porosities are getting filled slower which is likely due to their larger volume and smaller surface contact with the powder matrix that plays the role of a liquid reservoir. These mechanisms have been highlighted and their speed has been quantified.

3D observations have brought more details on the filling sequence. The different steps have been classified according to their duration, filling mechanisms and trigger. Multi directionnal progressions have been spotted as well as the filling of distinct porosities such as intra yarn, matrix/yarns decohesions and macropores. The continuity of the powder matrix is now known to play a significant role in the speed of filling. In addition, this work has proved that after saturation, the SiC matrix provides silicon for larger scale porosities that are filled more or less rapidly depending on their volume and surface contact.

This work is the first-ever proof-of-concept for 3D in-situ monitoring of silicon infiltration in CMC. This approach allowed to demonstrate mechanisms that could only be attainable through volume observation. The obtained 3D tomographic in situ observations of the high temperature capillary infiltration could give valuable insights for SiC/SiC composite manufacturing in order to reach complete saturation during the LSI process.

While this initial study faced limitations in image quality, preventing full utilization of the method, including Digital Volume Correlation (DVC) for accessing local volume changes and high-fidelity segmentation for detailed microstructure analysis, there is significant potential for future advancements. Improved image quality could pave the way for a comprehensive 3D image-based capillary infiltration model.

6 Acknowledgments

The authors wish to acknowledge SOLEIL for provision of synchrotron facilities and we would like to warmly thank all PSICHE beamline members for their kind assistance. We also thank Sebastien

Couthures, Théo Veyer, André Ebel from the Laboratory of Thermo Structural Composites (LCTS - UMR 5801 - UBCNRS- CEA-SAFRAN) for their help throughout the entire setup development. We are also very grateful for the advices given by Francisco García-Moreno about the rotation setup. Safran Ceramics company is thanked for the funding of the PhD that gave rise to these in situ experiments.

References

[1] W. Krenkel, "Design of High Preformance CMC Brake Discs," *Key Engineering Materials - KEY ENG MAT*, vol. 164–165, pp. 421–424, Jan. 1999.

[2] F. Christin, "Design, Fabrication, and Application of Thermostructural Composites (TSC) like C/C, C/SiC, and SiC/SiC Composites," *Advanced Engineering Materials*, vol. 4, pp. 903–912, Dec. 2002.

[3] R. Naslain, "Design, preparation and properties of non-oxide CMCs for application in engines and nuclear reactors: An overview," *Composites Science and Technology*, vol. 64, pp. 155–170, Feb. 2004.

[4] P. E. Gray, "Melt Infiltration of Ceramic Matrix Composites," p. 5, 2006.

[5] E. O. Einset, "Analysis of reactive melt infiltration in the processing of ceramics and ceramic composites," *Chemical Engineering Science*, vol. 53, pp. 1027–1039, Feb. 1998.

[6] S. Kumar, A. Kumar, R. Devi, A. Shukla, and A. Gupta, "Kumar et al. - 2009 - Capillary infiltration studies of liquids into 3D Part B: Kinetics of silicon infiltration," *Journal of the European Ceramic Society*, vol. 29, pp. 2651–2657, Sept. 2009.

[7] A. Marchais, *Etude des mécanismes de montée capillaire du silicium liquide au sein d'une préforme en carbure de silicium*. PhD thesis, Université de Bordeaux, 2016.

[8] J. Roger, L. Guesnet, A. Marchais, and Y. Le Petitcorps, "SiC/Si composites elaboration by capillary infiltration of molten silicon," *Journal of Alloys and Compounds*, vol. 747, pp. 484–494, May 2018.

[9] A. Marchais, J. Roger, and Y. Le Petitcorps, "Capillary infiltration of hexadecane in packed SiC powder and in SiC/SiC preforms: Pore description and calculation of molten Si infiltration," *Ceramics International*, vol. 42, pp. 7774–7780, May 2016.

[10] J. Roger, M. Avenel, and L. Lapuyade, "Characterization of SiC ceramics with complex porosity by capillary infiltration: Part B – Filling by molten silicon at 1500 °C," *Journal of the European Ceramic Society*, vol. 40, pp. 1869–1876, May 2020.

[11] N. M. Larson and F. W. Zok, "In-situ 3D visualization of composite microstructure during polymer-to-ceramic conversion," *Acta Materialia*, vol. 144, pp. 579–589, Feb. 2018.

[12] N. M. Larson and F. W. Zok, "Insights from in-situ X-ray computed tomography during axial impregnation of unidirectional fiber beds," *Composites Part A: Applied Science and Manufacturing*, vol. 107, pp. 124–134, Apr. 2018.

[13] N. M. Larson, C. Cuellar, and F. W. Zok, "X-ray computed tomography of microstructure evolution during matrix impregnation and curing in unidirectional fiber beds," *Composites Part A: Applied Science and Manufacturing*, vol. 117, pp. 243–259, Feb. 2019.

[14] E. Maire, C. Le Bourlot, J. Adrien, A. Mortensen, and R. Mokso, "20 Hz X-ray tomography during an in situ tensile test," *International Journal of Fracture*, vol. 200, pp. 3–12, July 2016.

[15] F. García-Moreno, P. H. Kamm, T. R. Neu, and J. Banhart, "Time-resolved *in situ* tomography for the analysis of evolving metal-foam granulates," *Journal of Synchrotron Radiation*, vol. 25, pp. 1505–1508, Sept. 2018.

[16] F. García-Moreno, P. H. Kamm, T. R. Neu, F. Bülk, R. Mokso, C. M. Schlepütz, M. Stampanoni, and J. Banhart, "Using X-ray tomoscopy to explore the dynamics of foaming metal," *Nature Communications*, vol. 10, p. 3762, Dec. 2019.

[17] V. Mazars, O. Caty, G. Couégnat, A. Bouterf, S. Roux, S. Denneulin, J. Pailhès, and G. L. Vignoles, "Damage investigation and modeling of 3D woven ceramic matrix composites from X-ray tomography in-situ tensile tests," *Acta Materialia*, vol. 140, pp. 130–139, Nov. 2017.

[18] L. Turpin, S. Roux, O. Caty, and S. Denneulin, "Coupling tomographic and thermographic measurements for in-situ thermo-mechanical tests," *Measurement Science and Technology*, vol. 32, p. 035401, Mar. 2021.

[19] S. Youssef, H. Deschamps, J. Dautriat, E. Rosenberg, R. Oughanem, E. Maire, and R. Mokso, "4D imaging of fluid flow dynamics in natural porous media with ultra-fast x-ray microtomography," p. 12, 2013.

[20] H. Carpentier, O. Caty, Y. Le Petitcorps, E. Maire, A. Marchais, N. Eberling-Fux, and G. Couégnat, "In situ observation of the capillary infiltration of molten silicon in a SiC/SiC composite by X-ray radiography," *Journal of the European Ceramic Society*, vol. 42, pp. 1947–1954, May 2022.

[21] K. L. Luthra and G. S. Corman, "Melt infiltrated (MI) SiC/SiC composites for gas turbine applications," in *High Temperature Ceramic Matrix Composites*, pp. 744–753, John Wiley & Sons, Ltd, 2006.

[22] B. Drevet and N. Eustathopoulos, "Wetting of ceramics by molten silicon and silicon alloys: A review," *Journal of Materials Science*, vol. 47, pp. 8247–8260, Dec. 2012.

[23] A. King, N. Guignot, P. Zerbino, E. Boulard, K. Desjardins, M. Bordessoule, N. Leclerq, S. Le, G. Renaud, M. Cerato, M. Bornert, N. Lenoir, S. Delzon, J.-P. Perrillat, Y. Legodec, and J.-P. Itié, "Tomography and imaging at the PSICHE beam line of the SOLEIL synchrotron," *Review of Scientific Instruments*, vol. 87, p. 093704, Sept. 2016.

[24] A. King, N. Guignot, J.-P. Deslandes, M. Pelerin, I. Joosten, D. De Looff, J. Li, L. Bertrand, E. Rosenberg, A. Dewaele, E. Boulard, Y. Le Godec, J.-P. Perrillat, E. Giovenco, G. Morard, T. Weitkamp, M. Scheel, J. Perrin, H. Chevreau, and J.-P. Itié, "Recent Tomographic Imaging Developments at the PSICHE Beamline," *Integrating Materials and Manufacturing Innovation*, vol. 8, pp. 551–558, Dec. 2019.

[25] A. Mirone, E. Brun, E. Gouillart, P. Tafforeau, and J. Kieffer, "The PyHST2 hybrid distributed code for high speed tomographic reconstruction with iterative reconstruction and a priori knowledge capabilities," *Nuclear Instruments and Methods in Physics Research Section B: Beam Interactions with Materials and Atoms*, vol. 324, pp. 41–48, Apr. 2014.

[26] S. van der Walt, J. L. Schönberger, J. Nunez-Iglesias, F. Boulogne, J. D. Warner, N. Yager, E. Gouillart, and T. Yu, "Scikit-image: Image processing in Python," *PeerJ*, vol. 2, p. e453, June 2014.

[27] F. Hild and S. Roux, "Comparison of Local and Global Approaches to Digital Image Correlation," *Experimental Mechanics*, vol. 52, pp. 1503–1519, Nov. 2012.

[28] A. Mendoza, J. Schneider, E. Parra, E. Obert, and S. Roux, "Differentiating 3D textile composites: A novel field of application for Digital Volume Correlation," *Composite Structures*, vol. 208, pp. 735–743, Jan. 2019.

[29] J. Roger, M. Avenel, and L. Lapuyade, "Characterization of SiC ceramics with complex porosity by capillary infiltration: Part A - Filling by hexadecane at 20 °C," *Journal of the European Ceramic Society*, vol. 40, pp. 1859–1868, May 2020.

[30] H. Carpentier, *Compréhension Des Mécanismes de Montée Capillaire Du Silicium Liquide Au Sein d'un Matériau Composite SiC(Fibres)/SiC(Matrice).* PhD thesis, 2021.

[31] Y. Wielhorski, A. B. Abdelwahed, and J. Bréard, "Theoretical Approach of Bubble Entrapment Through Interconnected Pores: Supplying Principle," *Transport in Porous Media*, vol. 96, pp. 105–116, Jan. 2013.

[32] Chung Hae Park and L. Woo, "Modeling void formation and unsaturated flow in liquid composite molding processes: A survey and review," *Journal of Reinforced Plastics and Composites*, vol. 30, pp. 957–977, June 2011.

[33] E. W. Washburn, "The Dynamics of Capillary Flow," *Physical Review*, vol. 17, pp. 273–283, Mar. 1921.